Published in final edited form as:
Eur J Nucl Med Mol Imaging. 2007 November ; 34(11): 1823–1831. doi:10.1007/s00259-007-0427-0.

^{18}F-labeled mini-PEG spacered RGD dimer (^{18}F-FPRGD2): synthesis and microPET imaging of $\alpha_v\beta_3$ integrin expression

Zhanhong Wu[#],
The Molecular Imaging Program at Stanford (MIPS), Department of Radiology and Bio-X Program, Stanford University School of Medicine, 1201 Welch Rd, P095, Stanford, CA 94305-5484, USA

Department of Nuclear Medicine, Peking Union Medical College Hospital, Beijing, People's Republic of China

Zi-Bo Li[#],
The Molecular Imaging Program at Stanford (MIPS), Department of Radiology and Bio-X Program, Stanford University School of Medicine, 1201 Welch Rd, P095, Stanford, CA 94305-5484, USA

Weibo Cai,
The Molecular Imaging Program at Stanford (MIPS), Department of Radiology and Bio-X Program, Stanford University School of Medicine, 1201 Welch Rd, P095, Stanford, CA 94305-5484, USA

Lina He,
The Molecular Imaging Program at Stanford (MIPS), Department of Radiology and Bio-X Program, Stanford University School of Medicine, 1201 Welch Rd, P095, Stanford, CA 94305-5484, USA

Frederick T. Chin,
The Molecular Imaging Program at Stanford (MIPS), Department of Radiology and Bio-X Program, Stanford University School of Medicine, 1201 Welch Rd, P095, Stanford, CA 94305-5484, USA

Fang Li, and
Department of Nuclear Medicine, Peking Union Medical College Hospital, Beijing, People's Republic of China

Xiaoyuan Chen
The Molecular Imaging Program at Stanford (MIPS), Department of Radiology and Bio-X Program, Stanford University School of Medicine, 1201 Welch Rd, P095, Stanford, CA 94305-5484, USA

[#] These authors contributed equally to this work.

shawchen@stanford.edu.

Electronic supplementary material The online version of this article (doi:10.1007/s00259-007-0427-0) contains supplementary material, which is available to authorized users.

Abstract

Purpose—We have previously reported that ^{18}F-FB-E[c(RGDyK)]$_2$ (^{18}F-FRGD2) allows quantitative PET imaging of integrin $\alpha_v\beta_3$ expression. However, the potential clinical translation was hampered by the relatively low radiochemical yield. The goal of this study was to improve the radiolabeling yield, without compromising the tumor targeting efficiency and in vivo kinetics, by incorporating a hydrophilic bifunctional mini-PEG spacer.

Methods—^{18}F-FB-mini-PEG-E[c(RGDyK)]$_2$ (^{18}F-FPRGD2) was synthesized by coupling *N*-succinimidyl-4-^{18}F-fluorobenzoate (^{18}F-SFB) with NH_2-mini-PEG-E[c(RGDyK)]$_2$ (denoted as PRGD2). In vitro receptor binding affinity, metabolic stability, and integrin $\alpha_v\beta_3$ specificity of the new tracer ^{18}F-FPRGD2 were assessed. The diagnostic value of ^{18}F-FPRGD2 was evaluated in subcutaneous U87MG glioblastoma xenografted mice and in c-*neu* transgenic mice by quantitative microPET imaging studies.

Results—The decay-corrected radiochemical yield based on ^{18}F-SFB was more than 60% with radiochemical purity of >99%. ^{18}F-FPRGD2 had high receptor binding affinity, metabolic stability, and integrin $\alpha_v\beta_3$-specific tumor uptake in the U87MG glioma xenograft model comparable to those of ^{18}F-FRGD2. The kidney uptake was appreciably lower for ^{18}F-FPRGD2 compared with ^{18}F-FRGD2 [2.0±0.2%ID/ g for ^{18}F-FPRGD2 vs 3.0±0.2%ID/g for ^{18}F-FRGD2 at 1 h post injection (p.i.)]. The uptake in all the other organs except the urinary bladder was at background level. ^{18}F-FPRGD2 also exhibited excellent tumor uptake in c-*neu* oncomice (3.6±0.1%ID/g at 30 min p.i.).

Conclusion—Incorporation of a mini-PEG spacer significantly improved the overall radiolabeling yield of ^{18}F-FPRGD2. ^{18}F-FPRGD2 also had reduced renal uptake and similar tumor targeting efficacy as compared with ^{18}F-FRGD2. Further testing and clinical translation of ^{18}F-FRGD2 are warranted.

Keywords

Integrin $\alpha_v\beta_3$; Dimeric RGD peptide; Mini-PEG spacer; MicroPET; Fluorine-18

Introduction

Members of the integrin family play vital roles in the regulation of cellular activation, migration, proliferation, survival, and differentiation. Integrin $\alpha_v\beta_3$ has been found to be highly expressed on osteoclasts and invasive tumors such as late-stage glioblastomas, breast and prostate tumors, malignant melanomas, and ovarian carcinomas [1, 2]. The expression level of integrin $\alpha_v\beta_3$ is an important factor in determining the invasiveness and metastatic potential of malignant tumors in both experimental tumor models and cancer patients [3, 4]. Therefore, non-invasive imaging of integrin $\alpha_v\beta_3$ expression using radiolabeled RGD-peptides may provide a unique means of characterizing the biological aggressiveness of a malignant tumor in an individual patient.

Cyclic arginine-glycine-aspartic acid (RGD) peptides bind to integrin $\alpha_v\beta_3$ and can inhibit new blood vessel formation, or angiogenesis [3]. ^{18}F labeling of cyclic RGD peptide was first reported by Haubner et al., and the tracer ^{18}F-galacto-RGD exhibited integrin $\alpha_v\beta_3$-

specific tumor uptake in the integrin-positive M21 melanoma xenograft model [5]. In the clinical setting, ^{18}F-galacto-RGD also showed tumor uptake in certain cancer patients, yet the standardized uptake values were suboptimal owing to the relatively low $\alpha_v\beta_3$ binding affinity of the monomeric RGD peptide and the imperfect pharmacokinetics [6]. Therefore, we and others have developed a series of dimeric and multimeric RGD peptides to improve the integrin $\alpha_v\beta_3$ targeting efficacy [7–19]. One tracer in particular, ^{18}F-fluorobenzoyl-E[c(RGDyK)]$_2$ (^{18}F-FB-E[c(RGDyK)]$_2$, denoted as ^{18}F-FRGD2, Fig. 1a), exhibited excellent integrin $\alpha_v\beta_3$-specific tumor imaging with favorable in vivo pharmacokinetics [9, 10]. The binding potential extrapolated from Logan plot graphical analysis of the positron emission tomography (PET) data correlated well with the receptor density measured by SDS-PAGE/autoradiography in various xenograft models. The tumor-to-background ratio at 1 h after injection of ^{18}F-FRGD2 also gave a good linear relationship with the tumor tissue integrin $\alpha_v\beta_3$ expression level [10]. However, the overall yield of ^{18}F-FRGD2 was not satisfactory, owing in part to the bulk of the two cyclic pentapeptides and the prosthetic group *N*-succinimidyl-4-^{18}F-fluorobenzoate (^{18}F-SFB). The glutamate α-amine group has a pK_a of 9.47, which is also less reactive than the ε-amino group on the lysine side chain (pK_a=8.95) usually used for ^{18}F labeling of peptides.

PEGylation has been widely used for improving the in vivo kinetics of various pharmaceuticals [20]. We have previously demonstrated that PEGylation of RGD peptides does improve the pharmacokinetics of the resulting tracers [8, 21, 22]. However, insertion of a long PEG also reduced the receptor binding affinity to some extent. In this study, we incorporated a mini-PEG spacer, 11-amino-3,6,9-trioxaundecanoic acid, with three ethylene oxide units, onto the glutamate α-amino group of the dimeric RGD peptide E[c (RGDyK)]$_2$ (denoted as RGD2). The hypothesis was that the mini-PEG will increase the overall hydrophilicity and alleviate the steric hindrance, thereby increasing the ^{18}F labeling yield. Since the spacer is quite short, such modification is not expected to significantly affect the receptor binding affinity or the in vivo kinetics of the tracer. The mini-PEG spacered dimeric RGD peptide was labeled with ^{18}F through ^{18}F-SFB and evaluated in murine tumor models by microPET imaging. Extensive in vitro, ex vivo, and in vivo experiments were carried out to evaluate the tumor targeting efficacy and pharmacokinetics of ^{18}F-FPRGD2, which was compared with the previously reported ^{18}F-FRGD2.

Materials and methods

All chemicals obtained commercially were of analytical grade and used without further purification. No-carrier-added ^{18}F-F$^-$ was obtained from an in-house PETtrace cyclotron (GE Healthcare). The semipreparative reversed-phase high-performance liquid chromatography (HPLC) system was the same as reported previously [10]. With a flow rate of 5 ml/min, the mobile phase was changed from 95% solvent A [0.1% trifluoroacetic acid (TFA) in water] and 5% solvent B [0.1% TFA in acetonitrile (ACN)] (0– 2 min) to 35% solvent A and 65% solvent B at 32 min. Analytical HPLC has the same gradient system except that the flow rate was 1 ml/min. The UV absorbance was monitored at 218 nm and the identification of the peptides was confirmed based on the UV spectrum acquired using a PDA detector. C_{18} Sep-Pak cartridges (Waters) were pretreated with ethanol and water before use.

Synthesis of NH_2-mini-PEG-E[c(RGDyK)]$_2$

To a solution of 40 mg (0.13 mmol) Boc-11-amino-3,6,9-trioxaundecanoic acid (Boc-NH-mini-PEG-COOH) and 20 μl *N*,*N*′-diisopropylethylamine (DIPEA) in ACN was added *O*-(*N*-succinimidyl)-1,1,3,3-tetramethyl-uronium tetrafluoroborate (TSTU, 27 mg, 0.09 mmol). The reaction mixture was stirred at room temperature for 0.5 h and then added to 25 mg (0.02 mmol) of E[c(RGDyK)]$_2$ in *N*,*N*′-dimethylformamide (DMF). After being stirred at room temperature for 2 h, the desired product Boc-NH-mini-PEG-E[c(RGDyK)]$_2$ was isolated by semipreparative HPLC. The Boc group was then removed with anhydrous TFA and the crude product was again purified by semi-preparative HPLC. The collected fractions were combined and lyophilized to afford NH_2-mini-PEG-E[c(RGDyK)]$_2$ (abbreviated as PRGD2) as a white fluffy powder.

Synthesis of FB-NH-mini-PEG-E[c(RGDyK)]$_2$

SFB (4 mg, 16.8 μmol) and PRGD2 (2 mg, 1.3 μmol) were mixed in 0.05 mol/l borate buffer (pH 8.5) at room temperature. After constant shaking for 2 h, the desired product FB-NH-mini-PEG-E[c(RGDyK)]$_2$ (abbreviated as FPRGD2) was isolated by semipreparative HPLC.

Cell binding assay

In vitro integrin $\alpha_v\beta_3$ binding affinity and specificity of PRGD2 and FPRGD2 were assessed via a competitive cell binding assay using ^{125}I-echistatin as the integrin $\alpha_v\beta_3$-specific radioligand [11, 13]. Experiments were performed on U87MG human glioblastoma cells with triplicate samples, as previously reported. The best-fit 50% inhibitory concentration (IC_{50}) values for the U87MG cells were calculated by fitting the data with non-linear regression using Graph-Pad Prism (GraphPad Software, Inc.) and compared with those of RGD2 and FRGD2.

Radiochemistry

^{18}F-SFB was synthesized as previously reported with HPLC purification [21, 23]. Recently, we incorporated ^{18}F-SFB synthesis into a commercially available synthetic module (TRACERlab FX_{FN}; GE) with automatic computer control. The purified ^{18}F-SFB was rotary evaporated to dryness, redissolved in dimethyl sulfoxide (DMSO, 200 μl), and added to a DMSO solution of PRGD2 (200 μg, 0.12 μmol) and DIPEA (20 μl). The reaction mixture was allowed to incubate at 60°C for 30 min. After dilution with 4 ml of water with 0.1% TFA, the mixture was injected onto the semipreparative HPLC. The collected fractions containing ^{18}F-FPRGD2 (Fig. 1b) were combined and rotary evaporated to remove ACN and TFA. The activity was then reconstituted in normal saline and passed through a 0.22-μm Millipore filter into a sterile multidose vial for in vivo experiments.

Octanol–water partition coefficient

Approximately 111 kBq of ^{18}F-FPRGD2 in 500 μl of PBS (pH 7.4) was added to 500 μl of octanol in an Eppendorf microcentrifuge tube. The mixture was vigorously vortexed for 1 min at room temperature. After centrifugation at 12,500 rpm for 5 min in an Eppendorf

microcentrifuge, 100-μl aliquots of both layers were pipetted and the radioactivity was measured using a gamma counter (Packard). The experiment was carried out in triplicates.

Cell line and animal models

U87MG cells were grown in Dulbecco's medium (Gibco) supplemented with 10% fetal bovine serum (FBS), 100 IU/ ml penicillin, and 100 μg/ml streptomycin (Invitrogen Co.), at 37°C in a humidified atmosphere containing 5% CO_2. All animal experiments were performed under a protocol approved by Stanford's Administrative Panel on Laboratory Animal Care. The subcutaneous U87MG tumor model was generated by injection of 5×10^6 cells in 50 μl PBS into the shoulder of female athymic nude mice (Harlan, Indianapolis, IN). The mice were subjected to microPET studies when the tumor volume reached 100–300 mm^3 (3–4 weeks after inoculation) [24, 25]. The c-*neu* oncomouse (Charles River Laboratories, Charles River, Canada) is a spontaneous tumor-bearing model that carries an activated c-*neu* oncogene driven by a mouse mammary tumor virus (MMTV) promoter [26]. Transgenic mice uniformly expressing the MMTV/c-*neu* gene develop mammary adenocarcinomas between 4 and 8 months postpartum that involve the entire epithelium in each gland. These mice were subjected to microPET scans at about 8 months old, when the tumor volume was about 300–500 mm^3.

MicroPET imaging

PET scans and image analysis were performed using a microPET R4 rodent model scanner (Siemens Medical Solutions) as previously reported [10, 11]. Each mouse was tail vein injected with about 3.7 MBq (100 μCi) of ^{18}F-FRGD2 under isoflurane anesthesia. The 30-min dynamic scan (1×30 s, 4×1 min, 1×1.5 min, 4×2 min, 1×2.5 min, 4×3 min, total of 15 frames) was started 1 min after injection. Five-minute static PET images were also acquired at 1 h and 2 h post injection (p.i.). The images were reconstructed by a two-dimensional ordered-subsets expectation maximum (OSEM) algorithm and no correction was applied for attenuation or scatter. For the blocking experiment, the tumor mice were co-injected with 10 mg/kg mouse body weight of c(RGDyK) and 3.7 MBq of ^{18}F-FPRGD2, and 5-min static PET scans were then acquired at 1 h p.i.

Metabolic stability of ^{18}F-FPRGD2

A U87MG tumor mouse was intravenously injected with 3.7 MBq of ^{18}F-FPRGD2. At 1 h after injection, the mouse was sacrificed, the blood, urine, liver, kidneys, and U87MG tumor were collected, and metabolite analysis was carried out as previously reported [10, 13]. In brief, blood sample was immediately centrifuged for 5 min at 13,200 rpm. Other tissues were homogenized and then centrifuged for 5 min at 13,200 rpm. Each supernatant was passed through a C_{18} Sep-Pak cartridge. The urine sample was directly diluted with 1 ml of PBS and passed through a C_{18} Sep-Pak cartridge. The cartridges were each washed with 2 ml of water and eluted with 2 ml of ACN containing 0.1% TFA. The ACN eluent was concentrated and injected onto the analytical HPLC. The eluent was collected with a fraction collector (0.5 min/fraction) and the radioactivity of each fraction was measured with the gamma counter.

Statistical analysis

Quantitative data were expressed as mean ± SD. Means were compared using one-way analysis of variance (ANOVA) and Student's *t* test. *P* values <0.05 were considered statistically significant.

Results

Chemistry

PRGD2 was synthesized with an overall yield of 64% (HPLC R_t: 12.2 min; MALDI-TOF-MS: $C_{67}H_{103}N_{20}O_{22}$, calculated 1,539.7, observed 1,540.1). FPRGD2 was prepared with 69% yield (HPLC R_t: 15.8 min; MALDI TOF-MS: $C_{74}H_{106}FN_{20}O_{23}$, calculated 1,662.7, observed 1,662.8).

The total time for ^{18}F-SFB synthesis was about 100 min and the decay-corrected yield was 67%±11% (n=10). The yield of ^{18}F-SFB coupling with PRGD2 is dependent on the peptide concentration, temperature, pH, solvent, and reaction time. After systematic investigation and optimization, 200 μg of PRGD2 was used for each reaction. The highest yield was achieved in DMSO with 20 μl DIPEA as the base. The decay-corrected radiochemical yield based on ^{18}F-SFB was more than 60% (*n*=3), significantly higher than the yield for ^{18}F-FRGD2 (maximum 23%, average 4 – 6%). The radiochemical purity of ^{18}F-FPRGD2 was >99% according to analytical HPLC and the specific activity was about 100–200 TBq/mmol based on the labeling agent ^{18}F-SFB, since the unlabeled PRGD2 was efficiently separated from the product. Starting from ^{18}F-F^-, the total synthesis time of ^{18}F-FPRGD2 was about 180 min and the overall decay-corrected yield was more than 40%. The much improved synthesis yield of ^{18}F-FPRGD2 makes it feasible for clinical translation. For example, starting from 37 GBq (1 Ci) of ^{18}F-F^-, about 4 – 5 GBq (100– 140 mCi) of ^{18}F-FPRGD2 can be synthesized in 3 h (enough for three to five patients).

The octanol/water partition coefficient (logP) for ^{18}F-FRGD2 was −2.28±0.05 (^{18}F-FRGD2: −2.10±0.03), indicating that the tracer is slightly more hydrophilic than ^{18}F-FRGD2 after incorporation of the mini-PEG spacer.

Cell binding assay

The receptor binding affinity of PRGD2 and FPRGD2 was evaluated using U87MG cells (integrin $\alpha_v\beta_3$ positive). Both peptides inhibited the binding of ^{125}I-echistatin (integrin $\alpha_v\beta_3$ specific) to U87MG cells in a concentration-dependent manner. The IC_{50} values for PRGD2 and FPRGD2 were 70.1±3.5 and 40.6±4.6 nmol/l (*n*=3) respectively, comparable to that of FRGD2 (55.1± 6.5 nmol/l). Owing to the presence of the mini-PEG linker and/or the prosthetic group (FB), all three peptides had slightly lower binding affinity than RGD2 (IC_{50}=26.1± 3.2 nmol/l). The comparable IC_{50} values of FRGD2 and FPRGD2 suggest that incorporation of a mini-PEG linker had minimal effect on the receptor binding. It is of note that cell-based receptor binding assay typically give higher IC_{50} values (lower binding affinity) than those measured by ELISA or solid-phase receptor binding assay. Therefore, when comparing the receptor binding affinity (IC_{50} values), it is critical that the IC_{50} values were obtained from the same assay.

MicroPET imaging study

Dynamic microPET scans were performed on the U87MG xenograft model, and selected coronal images at different time points after injecting ^{18}F-FPRGD2 are shown in Fig. 2a. High tumor uptake was observed as early as 5 min after injection. The U87MG tumor uptake was 4.9± 0.1, 3.4±0.3, and 2.7±0.1%ID/g at 30 min, 1 h, and 2 h p.i. respectively (n=3). Most activity in the non-targeted tissues and organs had been cleared by 1 h p.i. For example, the uptake values in the kidneys, liver, and lung were as low as 2.0±0.6, 1.1±0.3, and 0.5±0.2%ID/g, respectively, at 1 h p.i. For direct visual comparison, representative serial microPET images of U87MG tumor mice after injection of ^{18}F-FRGD2 are also shown (Fig. 2b). It can be seen that both tracers gave comparable imaging quality, indicating that the mini-PEG spacer did not significantly alter the tumor targeting efficacy in vivo. Because of the very low tracer uptake in most organs, especially in the abdominal region, ^{18}F-FPRGD2 is suitable for imaging integrin-positive lesions in most areas except for the kidneys and the urinary bladder. Time-activity curves showed that this tracer was excreted predominantly through the renal route (Fig. 3).

The integrin $\alpha_v\beta_3$ specificity of ^{18}F-FPRGD2 in vivo was confirmed by a blocking experiment where the tracer was co-injected with c(RGDyK) (10 mg/kg). As can be seen from Fig. 2c, the U87MG tumor uptake in the presence of non-radiolabeled RGD peptide (0.5±0.2%ID/g) was significantly lower than that without RGD blocking (3.4±0.3%ID/g) (p<0.001). As in a previous report [13], the tracer cleared from the body significantly faster and the uptake in most organs (e.g., kidneys and liver) was also lower than that without c(RGDyK) blocking. Western blot and immunohistochemical staining also confirmed that these organs express integrin $\alpha_v\beta_3$ (data not shown).

MicroPET imaging of c-*neu* oncomice with ^{18}F-FPRGD2

The c-*neu* oncomouse, a spontaneous tumor model which is more clinically relevant than the U87MG xenograft model, was also injected with ^{18}F-FPRGD2 and scanned in the microPET scanner (Fig. 2d). This spontaneous breast tumor has been well established in the literature to be integrin $\alpha_v\beta_3$ positive [27–30]. The spontaneous tumor uptake at 30 min p.i. was 3.6±0.1%ID/g (n=2), slightly higher than the kidney uptake (3.1±0.5%ID/g). The non-specific uptake in all the other organs was at background level (<1.5%ID/g). The tumor uptake dropped to 2.4±0.1%ID/g at 1 h p.i. Successful imaging of this spontaneous tumor model suggests the usefulness of ^{18}F-FPRGD2 in detecting integrin $\alpha_v\beta_3$-positive lesions in clinical settings.

Comparison of ^{18}F-FPRGD2 and ^{18}F-FRGD2

The comparison of uptake in tumor and various organs of ^{18}F-FPRGD2 and ^{18}F-FRGD2 is shown in Fig. 4. The uptake in the U87MG tumor was essentially the same, indicating that the two tracers have similar integrin $\alpha_v\beta_3$ binding affinity and targeting efficacy in vivo (Fig. 4a). The kidney uptake was lower for ^{18}F-FPRGD2 (Fig. 4b), with 2.7±0.2, 2.0±0.2, and 1.3±0.2%ID/g at 30 min, 1 h, and 2 h p.i. respectively; for ^{18}F-FRGD2, the kidney uptake was 3.6±0.1, 3.0±0.2, and 2.8±0.3%ID/g at 30 min, 1 h, and 2 h p.i. respectively. The liver uptake was similar for ^{18}F-FPRGD2 and ^{18}F-FRGD2 (Fig. 4c). The non-specific uptake in the muscle was slightly higher for ^{18}F-FPRGD2 at early time points (e.g., 30 min

p.i.), yet for both tracers, uptake was at a very low level (<0.5%ID/g, Fig. 4d) at 1 h p.i. Taken together, ^{18}F-FPRGD2 had similar tumor, liver, and non-specific uptake to ^{18}F-FRGD2, while the kidney uptake was appreciably lower.

Metabolic stability of ^{18}F-FPRGD2

The metabolic stability of ^{18}F-FPRGD2 was determined in mouse blood and urine samples and in the liver, kidneys, and U87MG tumor homogenates at 1 h p.i. (Table 1). After centrifugation of the tissue homogenates, the majority of the injected radioactivity (75–95%) was in the supernatant (denoted as "extraction efficiency"), indicating successful recovery of the radiotracer from the mouse tissue. After passing the supernatant through C_{18} Sep-Pak cartridges, most of the radioactivity was trapped and the non-retained fraction was less than 30%. After ACN elution, the radioactivity of each sample was injected onto an analytical HPLC, and the HPLC chromatograms are shown in Fig. 5. The fraction of intact tracer (R_t: 15.8 min) was between 68% and 100% (Table 1). A minor metabolite peak was found at about 13–14 min for the blood and liver samples. No defluorination was observed throughout the study. The metabolic stability of ^{18}F-FPRGD2 was similar to that of ^{18}F-FRGD2 (percentage of intact tracer between 79% and 96%), demonstrating that the incorporation of the mini-PEG spacer did not change the stability of the tracer in vivo.

Discussion

We have labeled c(RGDyK) and E[c(RGDyK)]$_2$ with ^{18}F using ^{18}F-SFB as a prosthetic group [9, 10, 31]. ^{18}F-FB-RGD had good tumor-to-blood and tumor-to-muscle ratios but also had rapid tumor washout and unfavorable hepatobiliary excretion. Because the natural mode of interactions between integrin $\alpha_v\beta_3$ and RGD-containing proteins (e.g., vitronectin and fibronectin) involves multivalent binding sites, multimeric cyclic RGD peptides could improve the integrin $\alpha_v\beta_3$ binding affinity, thus leading to better targeting capability and higher cellular uptake through the integrin $\alpha_v\beta_3$-dependent endocytosis pathway [2, 14, 15, 32]. Indeed, ^{18}F-FRGD2 had twofold higher tumor uptake than the monomeric tracer ^{18}F-FB-RGD [9]. The dimeric RGD peptide tracer ^{18}F-FRGD2 also allowed for quantification of the integrin $\alpha_v\beta_3$ expression level in vivo, through either graphical analysis of dynamic PET scans (Logan plot) or the tumor-to-background ratio at 1 h p.i., when most of the non-specific binding had been cleared [10]. This property, along with the excellent imaging quality and the favorable in vivo kinetics, deserves clinical investigation in cancer patients. Unfortunately, the overall radiolabeling yield of ^{18}F-FRGD2 was rather low. We believe that the low yield might be attributable to the steric hindrance and the low reactivity of the glutamate α-amino group (pK_a 9.47). In order to increase the overall radiolabeling yield and facilitate clinical translation, a mini-PEG spacer (three ethylene oxide units) was inserted between α-amine of the glutamate in E[c (RGDyK)]$_2$ and ^{18}F-SFB.

It has been well established that PEG is a suitable polymer for the covalent modification of molecules for many pharmaceutical applications [20]. Based on our previous reports where PEGylated (MW 3,400) RGD peptides were labeled with different isotopes [8, 21, 22], long PEG chain did improve the pharmacokinetics but at the same time also reduced the receptor binding affinity. Another concern of PEGylation is the heterogeneity of the resulting

PEGylated compounds. Long-chain PEGs are mixtures of a broad range of different molecular weight compounds and polydispersity can create many problems in the characterization and quality control of the PEGylated compound. Reproducible production of PEGylated radiopharmaceuticals is quite difficult and is not amenable for clinical translation. We thus decided to use the mini-PEG spacer with a definite molecular structure instead of the long polymeric PEG linker, aiming to minimize the PEGylation effect on the receptor binding affinity, imaging quality, tumor uptake, and in vivo kinetics.

To achieve optimal radiolabeling yield we tested different reaction conditions (solvent, temperature, pH, ^{18}F-SFB/peptide ratio, reaction time, etc.). In our previous studies, the reaction between ^{18}F-SFB and E[c(RGDyK)]$_2$ was carried out in borate buffer (pH 8.5). Because of hydrolysis, there are several side products (^{18}F-FB and partially hydrolyzed species) that have a similar HPLC retention time to the desired product ^{18}F-FRGD2. The peaks of ^{18}F-FRGD2 and ^{18}F-FPRGD2 are both very close to that of ^{18}F-FB, which makes the HPLC purification of the desired product quite difficult. In this study, we found that in anhydrous organic solvent (DMSO), the decay-corrected yield of ^{18}F-FPRGD2 based on ^{18}F-SFB was more than 60%. The yield of ^{18}F-FRGD2 under the same condition was significantly lower.

Comparison of the PET imaging results for ^{18}F-FPRGD2 and ^{18}F-FRGD2 revealed that ^{18}F-FPRGD2 had comparable tumor uptake and non-specific muscle uptake, while the kidney uptake was appreciably lower. The residence time for kidneys (calculated on the basis of the serial PET imaging data) was 0.016 h and 0.029 h for ^{18}F-FPRGD2 and ^{18}FFRGD2, respectively. The shorter residence time is desirable as the kidney is the only organ with appreciable tracer uptake and is clearly the dose-limiting organ. The uptake of ^{18}F-FRGD2 in the other major organs (e.g., liver and intestine) is at a very low level (less than 1.5%ID/g at 1 h p.i.) and will unlikely cause any adverse effects. Whether this is true for ^{18}F-FPRGD2 remains to be tested in human patients.

In this report, we used ^{18}F-SFB for the peptide labeling via the amino group. To further improve the yield, other labeling strategies may also be explored. For ^{18}F labeling through the amino group at the N terminus or the lysine side chain, oxime formation and reductive amination using 4-^{18}F-fluorobenzaldehyde (^{18}F-FBA) [33, 34], imidation reaction using 3-^{18}F-fluoro-5-nitrobenzimidate (^{18}F-FNB) [35], photochemical conjugation using 4-azidophenacyl ^{18}F-fluoride (^{18}F-APF) [36], and alkylation reactions using 4-^{18}F-fluorophenacyl bromide (^{18}F-FPB) [35] have been reported previously. ^{18}F labeling of peptide or protein via the carboxylic acid group at the C terminus or glutamic/ aspartic acid side chain is less common and only a few reports exist [37]. We have previously reported the thiol-reactive synthon for thiolated RGD peptide labeling [13]. Although the reaction between the thiol-reactive synthon and the thiolated RGD peptides was virtually quantitative, the synthesis of the thiol-reactive synthon required significant effort and time. Recently, click chemistry has been applied for ^{18}F labeling [38]. Although the labeling of model peptides was accomplished in good yield, no in vivo PET data have been reported. Microfluidics has also been utilized for rapid and efficient synthesis of radiotracers, and such a strategy may be explored in the future for ^{18}F-SFB/ peptide coupling to minimize the amount of solvent used and further increase the overall yield [39].

The goal of this study was to optimize the ^{18}F labeling yield for the dimeric RGD peptide for clinical translation. The yield has been significantly improved (more than 60% vs 4–6% average) compared with our previous reports. Next, we shall further evaluate whether the PET imaging result of ^{18}F-FPRGD2 can allow for non-invasive quantification of integrin $\alpha_v\beta_3$ expression in vivo. Other studies such as human dosimetry estimation based on PET of primates, acute toxicity studies under GLP condition, and side-by-side comparison with other integrin $\alpha_v\beta_3$ imaging agents (e.g., ^{18}F-galacto-RGD [6] and ^{99m}Tc-NC100692 [40]) are also warranted.

Conclusion

^{18}F-FPRGD2 was found to have high activity accumulation in $\alpha_v\beta_3$ integrin-rich U87MG tumors and spontaneous mammary carcinoma after injection. Excellent image quality, high integrin $\alpha_v\beta_3$ binding affinity/specificity, and good metabolic stability comparable to ^{18}F-FRGD2 were all maintained after incorporation of the mini-PEG spacer (11-amino-3,6,9-trioxaundecanoic acid). Most importantly, the radiolabeling yield was significantly improved and the renal uptake was significantly lowered for ^{18}F-FPRGD2 compared with ^{18}F-FRGD2, all of which makes ^{18}F-FPRGD2 suitable for clinical PET applications.

Acknowledgments

This work was supported in part by National Institute of Biomedical Imaging and Bioengineering (NIBIB) (R21 EB001785), National Cancer Institute (NCI) (R21 CA102123, P50 CA114747, U54 CA119367, and R24 CA93862), Department of Defense (DOD) (W81XWH-04-1-0697, W81XWH-06-1-0665, W81XWH-06-1-0042, and DAMD17-03-1-0143), and a Benedict Cassen Postdoctoral Fellowship from the Education and Research Foundation of the Society of Nuclear Medicine (to W. Cai). We thank Dr. David W. Dick from the cyclotron facility for ^{18}F-F$^-$ production.

References

1. Hynes RO. Integrins: bidirectional, allosteric signaling machines. Cell. 2002; 110:673–87. [PubMed: 12297042]
2. Cai W, Chen X. Anti-angiogenic cancer therapy based on integrin $\alpha_v\beta_3$ antagonism. Anti-Cancer Agents Med Chem. 2006; 6:407–28.
3. Brooks PC, Clark RA, Cheresh DA. Requirement of vascular integrin $\alpha_v\beta_3$ for angiogenesis. Science. 1994; 264:569–71. [PubMed: 7512751]
4. Hood JD, Cheresh DA. Role of integrins in cell invasion and migration. Nat Rev Cancer. 2002; 2:91–100. [PubMed: 12635172]
5. Haubner R, Wester H-J, Weber WA, Mang C, Ziegler SI, Goodman SL, et al. Noninvasive imaging of $\alpha_v\beta_3$ integrin expression using ^{18}F-labeled RGD-containing glycopeptide and positron emission tomography. Cancer Res. 2001; 61:1781–5. [PubMed: 11280722]
6. Haubner R, Weber WA, Beer AJ, Vabuliene E, Reim D, Sarbia M, et al. Noninvasive visualization of the activated $\alpha_v\beta_3$ integrin in cancer patients by positron emission tomography and [^{18}F] galacto-RGD. PLoS Med. 2005; 2:e70. [PubMed: 15783258]
7. Janssen ML, Oyen WJ, Dijkgraaf I, Massuger LF, Frielink C, Edwards DS, et al. Tumor targeting with radiolabeled $\alpha_v\beta_3$ integrin binding peptides in a nude mouse model. Cancer Res. 2002; 62:6146–51. [PubMed: 12414640]
8. Chen X, Sievers E, Hou Y, Park R, Tohme M, Bart R, et al. Integrin $\alpha_v\beta_3$-targeted imaging of lung cancer. Neoplasia. 2005; 7:271–9. [PubMed: 15799827]
9. Chen X, Tohme M, Park R, Hou Y, Bading JR, Conti PS. Micro-PET imaging of $\alpha_v\beta_3$-integrin expression with ^{18}F-labeled dimeric RGD peptide. Mol Imaging. 2004; 3:96–104. [PubMed: 15296674]

10. Zhang X, Xiong Z, Wu X, Cai W, Tseng JR, Gambhir SS, et al. Quantitative PET imaging of tumor integrin $\alpha_v\beta_3$ expression with ^{18}F-FRGD2. J Nucl Med. 2006; 47:113–21. [PubMed: 16391195]
11. Wu Y, Zhang X, Xiong Z, Cheng Z, Fisher DR, Liu S, et al. MicroPET imaging of glioma α_v-integrin expression using ^{64}Cu-labeled tetrameric RGD eptide. J Nucl Med. 2005; 46:1707–18. [PubMed: 16204722]
12. Cai W, Gambhir SS, Chen X. Multimodality tumor imaging targeting integrin $\alpha_v\beta_3$. Biotechniques. 2005; 39:S6–17. [PubMed: 20158503]
13. Cai W, Zhang X, Wu Y, Chen X. A thiol-reactive ^{18}F-labeling agent, N-[2-(4-^{18}F-fluorobenzamido)ethyl]maleimide (^{18}F-FBEM), and the synthesis of RGD peptide-based tracer for PET imaging of $\alpha_v\beta_3$ integrin expression. J Nucl Med. 2006; 47:1172–80. [PubMed: 16818952]
14. Haubner R. $\alpha_v\beta_3$-integrin imaging: a new approach to character-ise angiogenesis? Eur J Nucl Med Mol Imaging. 2006; 33(Suppl 11):54–63. [PubMed: 16791598]
15. Liu S. Radiolabeled multimeric cyclic RGD peptides as integrin $\alpha_v\beta_3$ targeted radiotracers for tumor imaging. Mol Pharm. 2006; 3:472–87. [PubMed: 17009846]
16. Ye Y, Bloch S, Xu B, Achilefu S. Design, synthesis, and evaluation of near infrared fluorescent multimeric RGD peptides for targeting tumors. J Med Chem. 2006; 49:2268–75. [PubMed: 16570923]
17. Thumshirn G, Hersel U, Goodman SL, Kessler H. Multimeric cyclic RGD peptides as potential tools for tumor targeting: solid-phase peptide synthesis and chemoselective oxime ligation. Chemistry. 2003; 9:2717–25. [PubMed: 12772286]
18. Watson N, Duncan G, Annan WS, van der Walle CF. A tetravalent RGD ligand for integrin-mediated cell adhesion. J Pharm Pharmacol. 2006; 58:959–66. [PubMed: 16805956]
19. Wester HJ, Kessler H. Molecular targeting with peptides or peptide-polymer conjugates: just a question of size? J Nucl Med. 2005; 46:1940–5. [PubMed: 16330555]
20. Harris JM, Chess RB. Effect of pegylation on pharmaceuticals. Nat Rev Drug Discov. 2003; 2:214–21. [PubMed: 12612647]
21. Chen X, Park R, Hou Y, Khankaldyyan V, Gonzales-Gomez I, Tohme M, et al. MicroPET imaging of brain tumor angiogenesis with ^{18}F-labeled PEGylated RGD peptide. Eur J Nucl Med Mol Imaging. 2004; 31:1081–9. [PubMed: 15118844]
22. Chen X, Hou Y, Tohme M, Park R, Khankaldyyan V, Gonzales-Gomez I, et al. Pegylated Arg-Gly-Asp peptide: ^{64}Cu labeling and PET imaging of brain tumor $\alpha_v\beta_3$-integrin expression. J Nucl Med. 2004; 45:1776–83. [PubMed: 15471848]
23. Cai W, Olafsen T, Zhang X, Cao Q, Gambhir SS, Williams LE, et al. PET imaging of colorectal cancer in xenograft-bearing mice by use of an 18F-labeled T84.66 anti–carcinoembryonic antigen diabody. J Nucl Med. 2007; 48:304–10. [PubMed: 17268029]
24. Cai W, Chen K, Mohamedali KA, Cao Q, Gambhir SS, Rosenblum MG, et al. PET of vascular endothelial growth factor receptor expression. J Nucl Med. 2006; 47:2048–56. [PubMed: 17138749]
25. Cai W, Wu Y, Chen K, Cao Q, Tice DA, Chen X. In vitro and in vivo characterization of ^{64}Cu-labeled Abegrin™, a humanized monoclonal antibody against integrin $\alpha_v\beta_3$. Cancer Res. 2006; 66:9673–81. [PubMed: 17018625]
26. Muller WJ, Sinn E, Pattengale PK, Wallace R, Leder P. Single-step induction of mammary adenocarcinoma in transgenic mice bearing the activated c-neu oncogene. Cell. 1988; 54:105–15. [PubMed: 2898299]
27. Harris TD, Kalogeropoulos S, Nguyen T, Dwyer G, Edwards DS, Liu S, et al. Structure-activity relationships of ^{111}In- and ^{99m}Tc-labeled quinolin-4-one peptidomimetics as ligands for the vitronectin receptor: potential tumor imaging agents. Bioconjug Chem. 2006; 17:1294–313. [PubMed: 16984141]
28. Onthank DC, Liu S, Silva PJ, Barrett JA, Harris TD, Robinson SP, et al. ^{90}Y and ^{111}In complexes of a DOTA-conjugated integrin $\alpha_v\beta_3$ receptor antagonist: different but biologically equivalent. Bioconjug Chem. 2004; 15:235–41. [PubMed: 15025518]

29. Harris TD, Kalogeropoulos S, Nguyen T, Liu S, Bartis J, Ellars C, et al. Design, synthesis, and evaluation of radiolabeled integrin $\alpha_v\beta_3$ receptor antagonists for tumor imaging and radiotherapy. Cancer Biother Radiopharm. 2003; 18:627–41. [PubMed: 14503959]
30. Mousa SA, Mohamed S, Wexler EJ, Kerr JS. Antiangiogenesis and anticancer efficacy of TA138, a novel $\alpha_v\beta_3$ antagonist. Anticancer Res. 2005; 25:197–206. [PubMed: 15816539]
31. Chen X, Park R, Shahinian AH, Tohme M, Khankaldyyan V, Bozorgzadeh MH, et al. 18F-labeled RGD peptide: initial evaluation for imaging brain tumor angiogenesis. Nucl Med Biol. 2004; 31:179–89. [PubMed: 15013483]
32. Boturyn D, Coll JL, Garanger E, Favrot MC, Dumy P. Template assembled cyclopeptides as multimeric system for integrin targeting and endocytosis. J Am Chem Soc. 2004; 126:5730–9. [PubMed: 15125666]
33. Poethko T, Schottelius M, Thumshirn G, Hersel U, Herz M, Henriksen G, et al. Two-step methodology for high-yield routine radiohalogenation of peptides: ^{18}F-labeled RGD and octreotide analogs. J Nucl Med. 2004; 45:892–902. [PubMed: 15136641]
34. Schottelius M, Poethko T, Herz M, Reubi JC, Kessler H, Schwaiger M, et al. First ^{18}F-labeled tracer suitable for routine clinical imaging of sst receptor-expressing tumors using positron emission tomography. Clin Cancer Res. 2004; 10:3593–606. [PubMed: 15173065]
35. Kilbourn MR, Dence CS, Welch MJ, Mathias CJ. Fluorine-18 labeling of proteins. J Nucl Med. 1987; 28:462–70. [PubMed: 3494825]
36. Wester HJ, Hamacher K, Stoecklin G. A comparative study of n.c.a. fluorine-18 labeling of proteins via acylation and photochemical conjugation. Nucl Med Biol. 1996; 23:365–72. [PubMed: 8782249]
37. Wilbur DS. Radiohalogenation of proteins: an overview of radionuclides, labeling methods and reagents for conjugate labeling. Bioconjug Chem. 1992; 3:432–70.
38. Marik J, Sutcliffe JL. Click for PET: rapid preparation of [^{18}F]fluoropeptides using CuI catalyzed 1,3-dipolar cycloaddition. Tetrahedron Lett. 2006; 47:6681–4.
39. Lee CC, Sui G, Elizarov A, Shu CJ, Shin YS, Dooley AN, et al. Multistep synthesis of a radiolabeled imaging probe using integrated microfluidics. Science. 2005; 310:1793–6. [PubMed: 16357255]
40. Bach-Gansmo T, Danielsson R, Saracco A, Wilczek B, Bogsrud TV, Fangberget A, et al. Integrin receptor imaging of breast cancer: a proof-of-concept study to evaluate ^{99m}Tc-NC100692. J Nucl Med. 2006; 47:1434–9. [PubMed: 16954550]

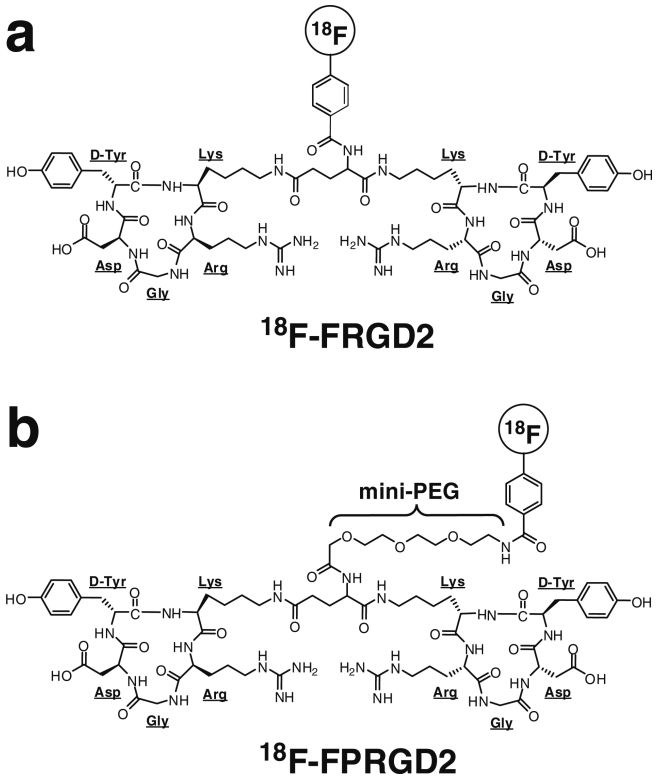

Fig. 1.

Chemical structures of ^{18}F-FRGD2 (**a**) and ^{18}F-FPRGD2 (**b**). The only difference between the two structures is the mini-PEG spacer

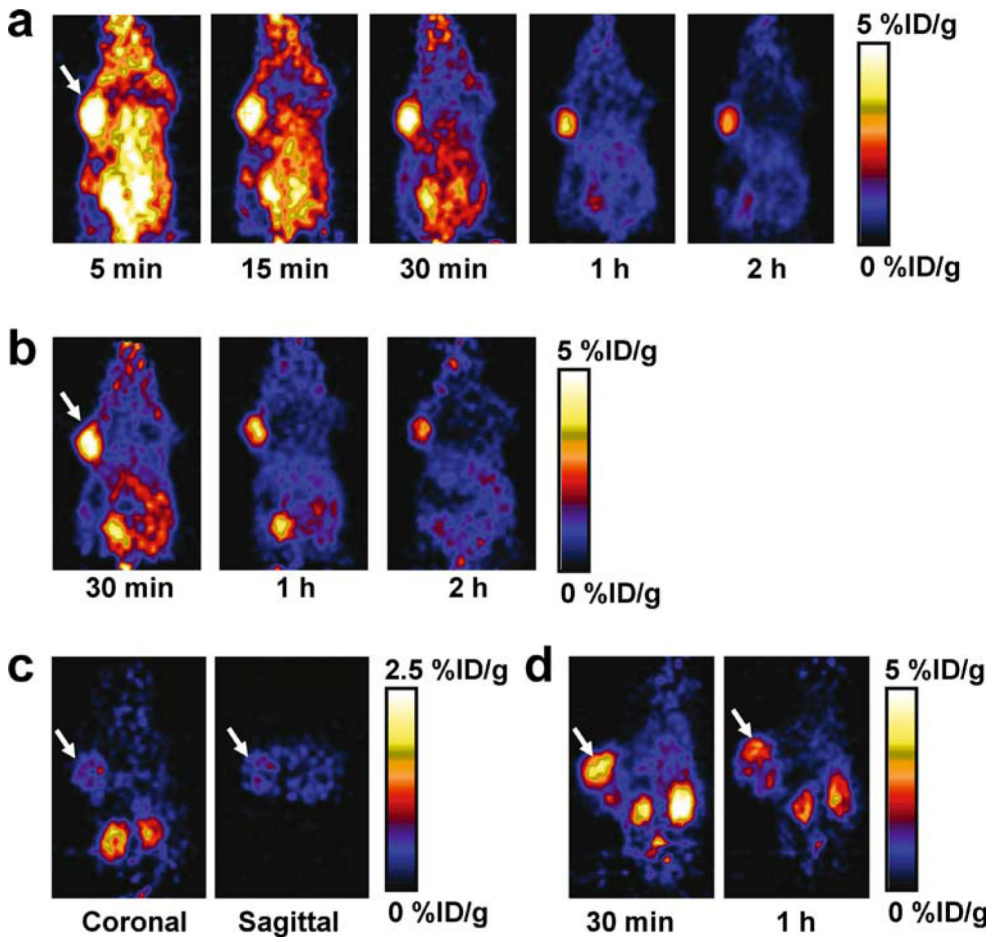

Fig. 2.

a Serial microPET images of U87MG tumor-bearing mice after intravenous injection of ^{18}F-FPRGD2. b For direct visual comparison, serial microPET images of U87MG tumor-bearing mice after intravenous injection of ^{18}F-FRGD2 are also shown. c Coronal and sagittal microPET images of a U87MG tumor-bearing mouse 1 h after co-injection of ^{18}F-FRGD2 and a blocking dose of c(RGDyK). Note that the scale (0–2.5%ID/g) is different from those in a and b (0–5%ID/g). d MicroPET images of a c-*neu* oncomouse after intravenous injection of ^{18}F-FPRGD2. *Arrows* indicate tumors in all cases

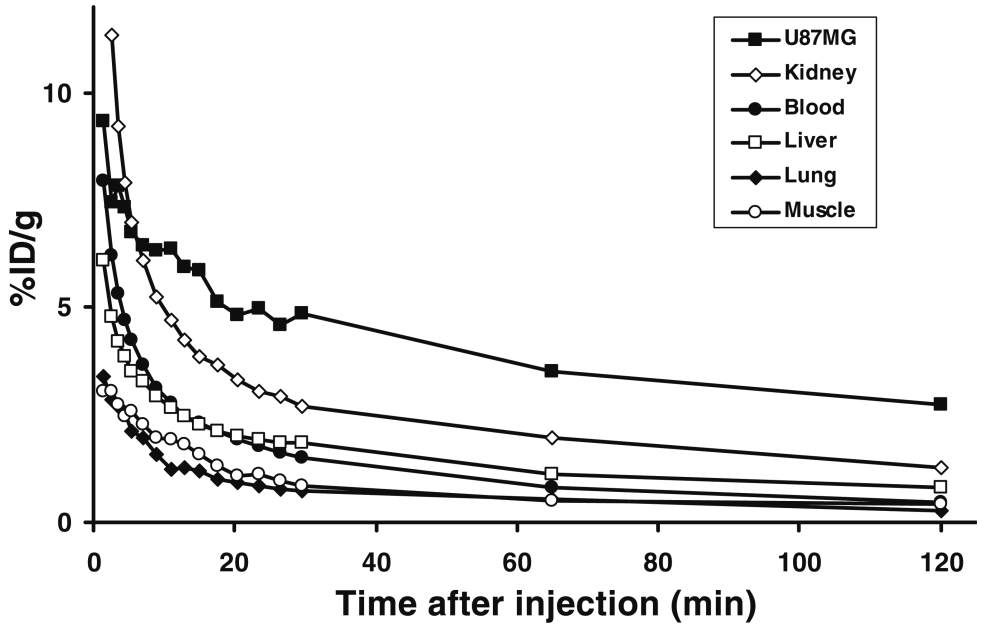

Fig. 3.
Time-activity curves of major organs after intravenous injection of ^{18}F-FPRGD2

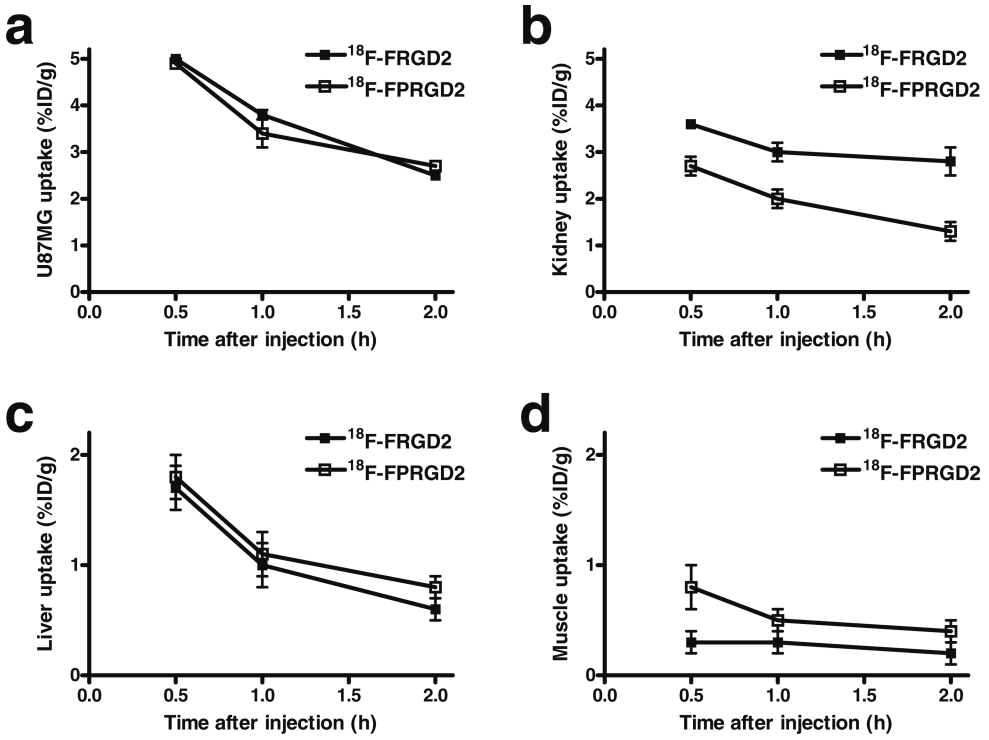

Fig. 4.

Comparison between ^{18}F-FRGD2 and ^{18}F-FPRGD2 in U87MG tumor (**a**), kidney (**b**), liver (**c**), and muscle (**d**) over time

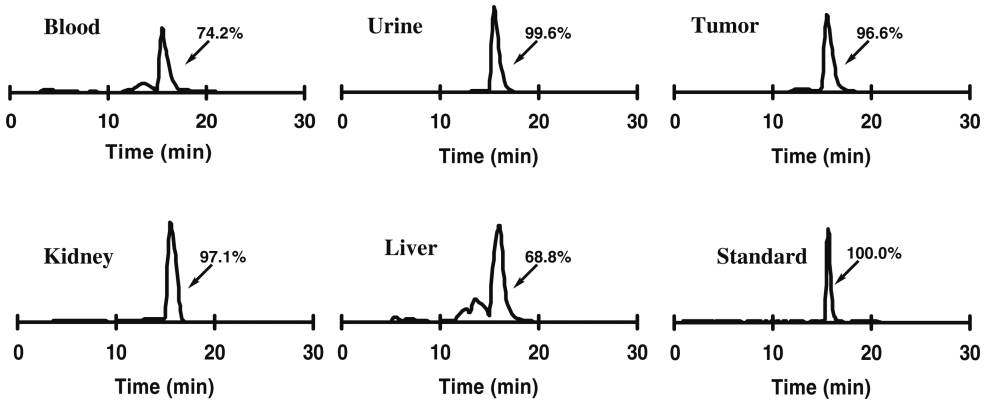

Fig. 5.

Metabolic stability of ^{18}F-FPRGD2 in mouse blood and urine samples and in liver, kidney, and U87MG tumor homogenates at 1 h after injection. The HPLC profile of pure ^{18}F-FPRGD2 (*Standard*) is also shown

Table 1

Extraction efficiency, elution efficiency, and HPLC analysis of soluble fractions of tissue homogenates at 1 h post injection of ^{18}F-FPRGD2

Fraction	Blood	Urine	Liver	Kidney	U87MG
Extraction efficiency (%)					
Insoluble fraction	5.2	ND	23.3	21.8	24.4
Soluble fraction	94.8	ND	76.7	78.2	75.6
Elution efficiency (%)					
Non-retained fraction	2.4	1.2	23.7	12.6	28.4
Wash water	1.2	0.2	4.3	2.0	4.3
Acetonitrile eluent	96.4	98.6	72.0	85.4	67.4
HPLC analysis (%)					
Intact tracer	74.2	99.6	68.8	97.1	96.6

ND not determined